ADVANCED FUNCTIONAL MATERIALS
www.afm-journal.de

Copper-Stabilized Sulfur-Microporous Carbon Cathodes for Li–S Batteries

Shiyou Zheng, Feng Yi, Zhipeng Li, Yujie Zhu, Yunhua Xu, Chao Luo, Junhe Yang, and Chunsheng Wang**

A copper-stabilized sulfur-microporous carbon (MC-Cu-S) composite is synthesized by uniformly dispersing 10% highly electronically conductive Cu nanoparticles into microporous carbon (MC), followed by wet-impregnating S. In the MC-Cu-S composite, the MC host that physically confines S/polysulfides provides free space to accommodate volumetric expansion of S during lithiation, while the Cu nanoparticles that are anchored in the MC further chemically interact with S/polysulfides through bonding between Cu and S/polysulfides. The Cu loading allows the S content to increase from 30 to 50% in the carbon-S cathode material without scarifying the electrochemical performance in a low-cost carbonate electrolyte. At a current density of 100 mA g^{-1}, the MC-Cu-S cathode shows that Coulumbic efficiency is close to 100% and capacity maintains more than 600 mAh g^{-1} with progressive cycling up to more than 500 cycles. In addition, the Cu nano-inclusins also enhance the electronic conductivity of the MC-Cu-S composite, remarkably increasing the rate capabilities. Even the current density increases 10.0 A g^{-1}, the MC-Cu-S cathode can still deliver a capacity of 200 mAh g^{-1}. This strategy of stabilization of S with small amount of metal nanoparticles anchored in MC provides an effective approach to improve the cycling stability, Coulumbic efficiency, and S loading for Li–S batteries.

1. Introduction

Lithium–sulfur (Li–S) batteries, which utilize elemental S as the active cathode material to reversibly react with Li, are considered to be a promising energy-storage solution for the rapidly growing hybrid electric vehicle and renewable energy. In addition, S is one of naturally abundant, low-cost and environmentally friendly elements. Assuming S can maximally interact with two Li atoms per S atom, the S cathode can provide reversible high capacity of 1675 mAh g^{-1} at average potentials of 2.0 V,[1–3] which is 10× higher energy density than that of classical commercial $LiCoO_2$ cathode. Since the capacity of current $LiCoO_2$-graphite Li-ion battery is controlled by $LiCoO_2$ cathode, replacement of expensive $LiCoO_2$ with cheap S will largely enhance the battery energy density. However, the S cathodes are still suffering from poor cycle life, high self-discharge, low Coulumbic efficiency and low overall capacity because of: i) low S utilization and low S loading arising from insulating nature of S;[4–6] ii) internal "shuttle reaction" induced by dissolution of lithium polysulfide intermediates (Li_2S_x, $4 \le x \le 8$) in liquid organic electrolytes and highly reactive of lithium polysulfide anions to carbonate solvent in carbonated electrolyte,[7,8] and iii) large volume change of S during lithiation/delithiation.[9,10] Current strategies to overcome these challenges focus on: 1) using carbon materials (microporous carbon,[11–16] carbon nanotubes,[17–19] graphene,[20–22] and carbon spheres.[23–26] and other conductive materials[27–29] to physically restrain polysulfides, facilitate electron transport and provide free-space to accommodate the volume change of S/polysulfides,[4,10] 2) adopting mesoporous silica as polysulfide intermediates absorber through weak bond to suppress the dissolution of polysulfides,[30] 3) preparing composites with small-chain S_2 to avert the formation of soluble high-order polysulfides,[16,17] and 4) employing different organic electrolytes to manipulate the solubility of S/polysulfides.[31–33] Although S encapsulated by porous carbon can significantly improve the S utilization and reduce the "shuttle reaction", the full electrochemical reversibility is hardly achieved, which leads to a gradual capacity deterioration upon cycling.[34–36] This is because the current technology for carbon encapsulation of S just reduces but not totally eliminates the "shuttle reaction". To avoid forming soluble high-order polysulfide (Li_2S_x, $4 \le x \le 8$) during charge/discharge, we prepared a microporous carbon-S composite by breaking cyclic molecules S_8 into a diatomic molecule S_2 and infusing the S_2 into porous carbon at high temperature, which largely increases the cycling stability and Coulumbic efficiency of S cathode.[16,17] However, the S loading is limited to around 30% in the microporous carbon-S composite due to the insulating nature of S_2, Li_2S_2, and Li_2S,

Prof. S. Zheng, Prof. J. Yang
School of Materials Science and Engineering
University of Shanghai for Science and Technology
Shanghai, 200093, China
E-mail: jhyang@usst.edu.cn
Dr. Y. Zhu, Dr. Y. Xu, Mr. C. Luo, Prof. C. Wang
Department of Chemical and Biomolecular Engineering
University of Maryland
College Park, MD 20742, USA
E-mail: cswang@umd.edu
Dr. F. Yi, Z. Li
Material Measurement Laboratory
National Institute of Standards and Technology
Gaithersburg, MD 20899, USA

DOI: 10.1002/adfm.201304156

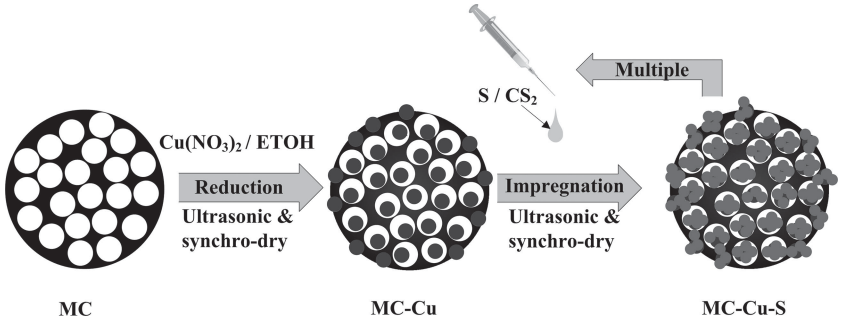

Scheme 1. Schematic drawing of preparation process for MC-Cu-S composite: Cu nanoparticles percolate through the MC and act as "anchor" to stabilize the S.

which leads to low overall capacity. It is well know that S and polysulfide intermediates are non-conductive and their electrochemical reactions can only occur when the S loading thickness on the conductive matrix is within electron tunnelling range. Therefore, how to increase the S utilization at high S loading with less "shuttle reaction" is one of key challenges in Li–S batteries. One attempt to solve the problem is to use a high soluble electrolyte for high-order polysulfides, that is, the polysulfide intermediates dissolving into this type liquid electrolyte at ease, which will continuously expose the inner S to the conductive carbon and drive the reaction forward. For instance, bis-(trifluoromethane)sulfonimide lithium (LiTFSI) in dimethoxyethane and dioxolane and tetra(ethylene glycol) dimethyl ether,[37–39] with high solubility to polysulfide are generally adopted in the Li–S cells. However, the dissolution of polysulfide intermediates will cause severe redox "shuttle reaction" and lead to poor cycle life, high self-discharge rate and low Coulumbic efficiency. Recently, Nazar et al reported a high loading S cathode by incorporating 70% S into bimodal mesoporous cabon. Due to the insulting nature and high loading of S, the high soluble and expensive ether-based electrolyte has to be used.[40] Thus, although the use of high-cost ether-based electrolyte in Li–S batteries can increase S loading, it also generates "shuttle reaction", reducing the cycle life and Coulumbic efficiency. On the other hand, it is a challenge to directly use the low-cost classical carbonate-based electrolytes due to the side reaction of dissolved polysulfide anions and carbonate solvents.

Alternative way to increase the S loading is to uniformly distribute thin-layer S in conductive materials through the strong interaction between S and conductive host. For instance, a stable and high capacity was reported for carbyne polysulfide prepared by co-heating polyvinylidene chloride and S in ammonia environment.[41] Also, Wang et al. reported that a polymer-S composite cathode synthesized by chemical reaction between polyacrylonitrile and S shows good cycle life and rate capability.[42] Transition metals (Co, Ni, and Cu, etc.) can react with S to form sulfides at moderate temperatures. These transition metal sulfides have been investigated as cathode materials for carbonate solvent-based Li–S batteries;[43–45] in particular, their nanoscale materials can be synthesized at a low temperature and meanwhile show fairly stable cycle life.[46,47] The strong bonds between metal and S allow the S in metal sulfides to directly form Li_2S and metal without forming soluble high-order polysulfide during lithiation. Due to the high atomic weight of transition metals, the specific capacities of these metal sulfides are low. However, if the transition metal nanoparticles or thin films are uniformly dispersed into porous carbon to absorb (but not alloy with) S and polysufides, the strong interaction between highly-conductive transition metals and S can stabilize and load more S in porous carbon. At same time, it has been reported that the carbyne polysulfide,[41] polymer-S and S_2/C composites with S bonding can stably charge/discharge in commercial carbonate-based electrolyte.[17,42] Therefore, if the metal-S bond can avoid the formation of high-order polysulfide during lithiation/delithiation, the carbonate-based electrolyte can be conveniently used to lower the cost.

Among these transition metals, Cu is a highly conductive, naturally abundant and low-cost element. It is also highly reactive with S as evidenced by the formation of CuS when coating S onto Cu foil at 60 °C and the formation of polysulfide clusters in a S-rich environment.[45,48] In this study, we report a rational design of copper-stabilized sulfur-microporous carbon (MC-Cu-S) composite with high S loading of 50% as a cathode for carbonate electrolyte Li–S batteries. An ultrasonic-assisted multiple wetness impregnation and synchro-dry technique was employed to introduce Cu and load S, as schematically demonstrated in **Scheme 1**. In the composite of MC-Cu-S, microporous structure of MC physical confines the S, while the Cu nanoparticles further act as "immobilizer" to weld S/polysulfides, thus more effectively reducing the active material loss upon prolonged cycling. The MC-Cu-S composite cathodes show stable, high and reversible capacities together with good rate and cycling capabilities even in conventional Li-ion battery electrolyte (1.0M $LiPF_6$ + EC/DEC (1 : 1 v/v)).

2. Results and Discussion

2.1. Structural Characterization

The surface morphologies of MC, MC-Cu composite, and MC-Cu-S composite are presented in **Figure 1**. The scanning electron microscopy (SEM) image of the MC shows a spherical shape with a particle size of about 500 nm (Figure 1a). After depositing with Cu or Cu and S, no change in the morphology can be observed from the MC-Cu or the MC-Cu-S SEM images (Figure 1b–d), indicating that the MC is a structural stable matrix supporting Cu and S. The energy dispersive X-ray spectrometry (EDS) elemental maps for the MC-Cu-S composite are also displayed in Figure 1e–h. Although the real distribution of carbon in the MC-Cu-S composite cannot be distinguished from the EDS map due to conductive carbon tape using in the SEM sample preparation, we can easily see that the Cu map follows the spherical skeleton of the MC matrix, and the S map coincides well with that of Cu. This suggests that both Cu and S are well dispersed in the MC-Cu-S composite.

The microstructures of MC, MC-Cu, and MC-Cu-S were further characterized by high resolution transmission electron

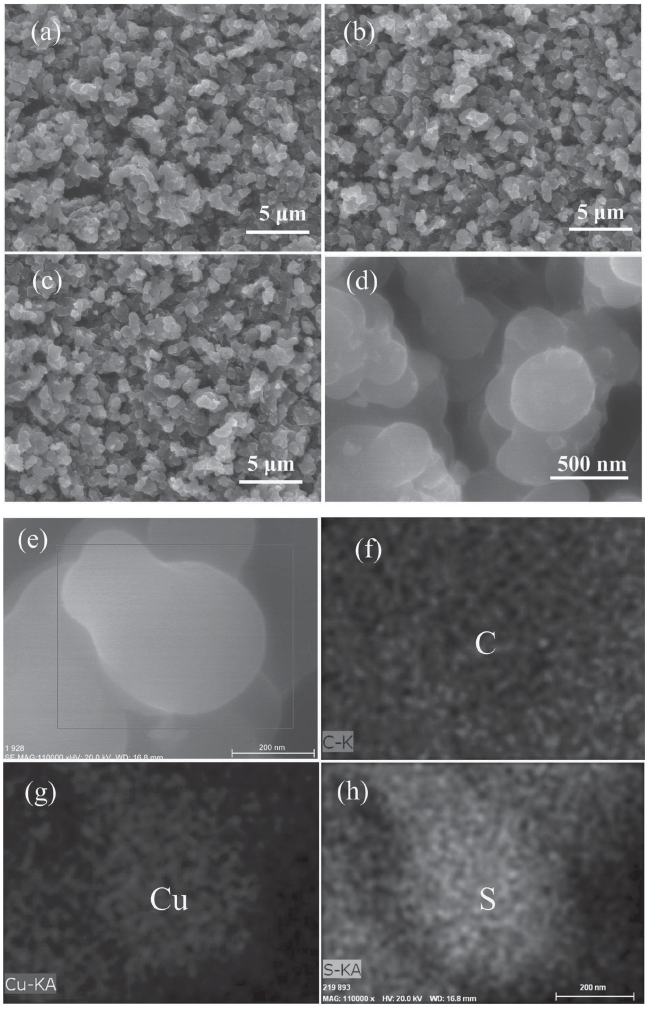

Figure 1. a) SEM image of the MC, b) SEM image of the MC-Cu, c) SEM image of the MC-Cu-S, d) enlarged SEM image of the MC-Cu-S, and the corresponding EDS maps of f) C, g) Cu, and h) S for image (e).

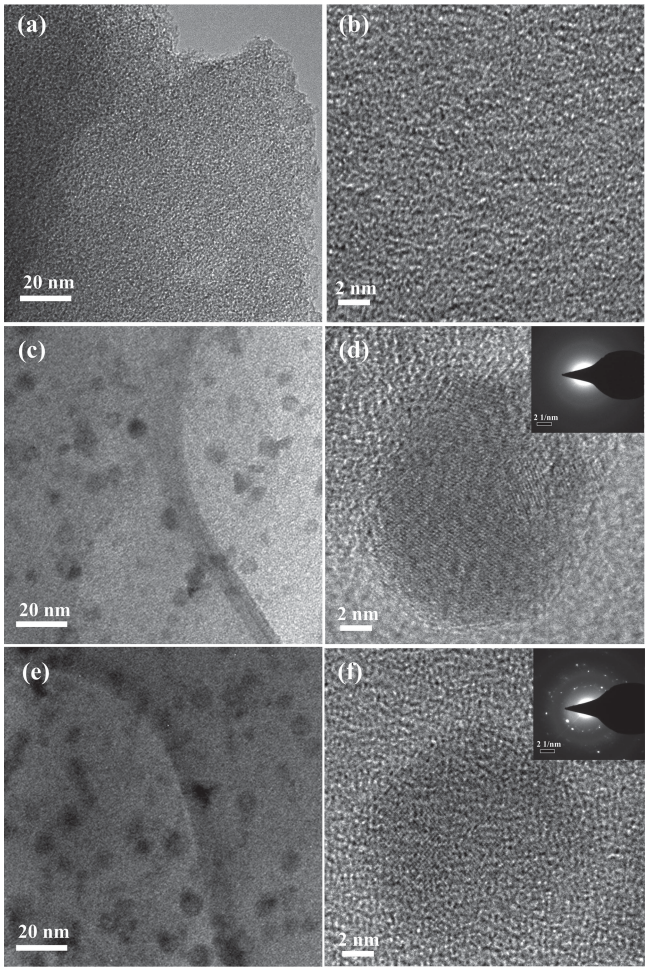

Figure 2. HRTEM images of a,b) the MC, c,d) the MC-Cu, and e,f) the MC-Cu-S.

microscopy (HRTEM) and selected area electron diffraction (SAED), as shown in **Figure 2**. From Figure 2a,b, a typical morphology of MC can be observed, but the pore size cannot be distinguished due to its overlapping distribution of pores.[23] After 10% of Cu loading, Cu nanoparticles with size around 3–6 nm are uniformly distributed in MC matrix (see Figure 2c). The lattice of Cu can be clearly observed in HRTEM in Figure 2d and confirmed by the SAED pattern inserted. S impregnation into MC matrix does not change the morphology of MC-Cu composite (Figure 2e,f). However, the SAED pattern of MC-Cu-S sample in inset of Figure 2f shows the clear rings made up of discrete spots, which may attribute to the formation of Cu-polysulfides CuS_x.

The phase structures of MC, Mixed MC-S, MC-S, MC-Cu and MC-Cu-S were characterized using X-ray diffraction (XRD) and displayed in **Figure 3**a. The XRD pattern of pristine MC only shows two broad peaks in the range of 20–50° (curve a), demonstrating that MC is an amorphous carbon. After physically mixing with S, the sharp and intense peaks from the crystalline S (S_8) can be clearly observed (curve b). While S was impregnated in the MC using S/CS_2-solution, the peaks of the crystalline S disappear (curve c), only the pattern of amorphous carbon is visible. The difference in XRD pattern between the Mixed MC-S and the impregnated MC-S demonstrated that the S is uniformly dispersed in MC matrix as an amorphous state and/or very fine crystallites when S is impregnated using the wetting impregnation method. When Cu is deposited into MC using ultrasonic-assisted multiple wetness impregnation and synchro-dry technique, Cu nanoparticles exist in crystal as demonstrated in the XRD peaks (curve d). Undergoing S impregnation into the MC-Cu material, Cu peaks disappear but few new peaks belonging to Cu-polysulfides CuS_x appear (curve e).[49] The XRD results confirm the occurrences of chemical bonding between Cu and S in the MC-Cu-S, which is in accordance with our expectation. These features indicate that the S is not just physically encapsulating in the nanoscale pores of carbon matrix, but chemically interacting with Cu nanoparticles in the MC-Cu-S composite. X-ray photoelectron spectroscopy (XPS) was used to further confirm the interaction between Cu and S. Figure 3b presents the survey scan and Cu 2p and S 2p binding energy spectra of MC-Cu-S composite. In the high-resolution Cu 2p spectrum, there exist four distinct

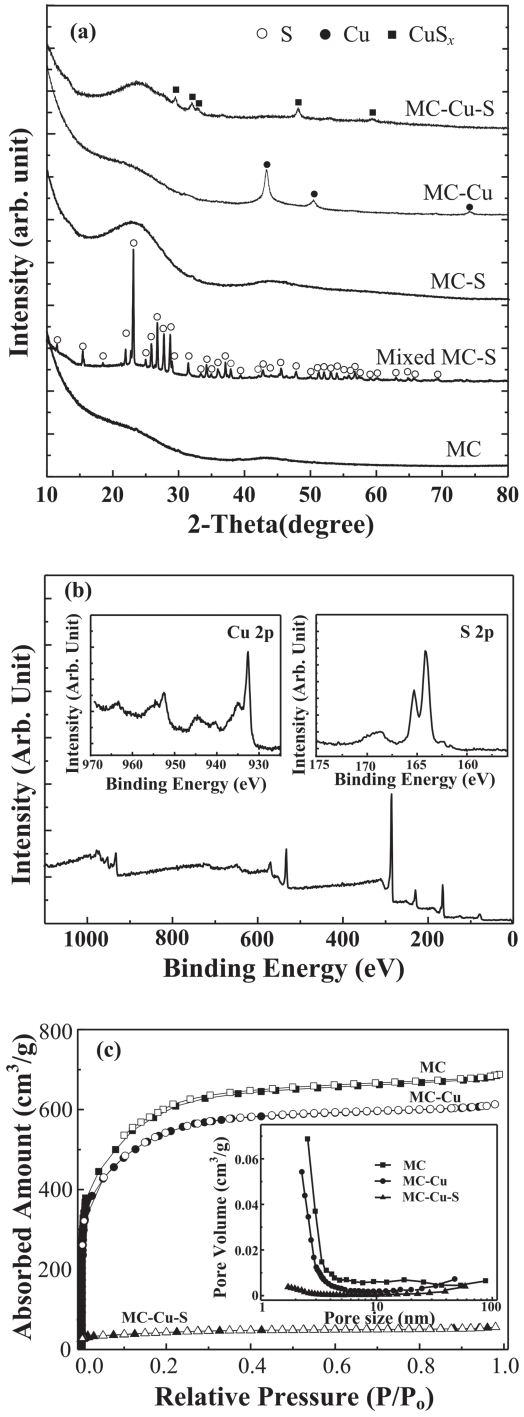

Figure 3. a) XRD patterns of MC, Mixed MC-S, MC-S, MC-Cu, and MC-Cu-S, b) XPS spectra of MC-Cu-S composite, with the insets showing the magnified Cu 2p and S 2p spectrum, respectively, c) N_2 adsorption isotherms of MC, MC-Cu, and MC-Cu-S and the corresponding pore size distributions (insert).

peaks at around 932.7 and 952.5 eV for Cu^{1+} 2p3/2 and 2p1/2 core levels, and 934.8 and 954.3 eV for Cu^{2+} 2p3/2 and 2p1/2 core levels, which reveal that the chemical valences of Cu in the MC-Cu-S composite are in mixture valence states of +1 and +2. Besides these main peaks, the "shake-up" satellites at ≈945 and ≈965 eV for the Cu 2p3/2 and 2p1/2 core levels are clearly visible, which provide an evidence of an open $3d^9$ shell of Cu(+2).[50,51] The S 2p spectrum shows three major peaks. The dual peaks positioned at 165.3 and 164.1 eV are assigned to S 2p1/2 and 2p3/2 due to spin orbit coupling, but the binding energies are slightly higher than those of the characteristic peaks of elemental S, indicating that the possible sulfur signal comes from the polysulfides CuS_x. In addition, the broad higher binding energy peak centered between 167 and 172 eV is observed, which proves the strong interaction between sulfur and copper.[52,53] The XPS results verify the formation of Cu-polysulfides CuS_x. Specific surface area, pore size distribution, and pore volume of MC, MC-Cu, and MC-Cu-S were measured using the N_2 adsorption-desorption isotherms. As shown in Figure 3c, the MC shows a typical isotherm of type I. The pore sizes (inserted in Figure 3c) are mainly in the range of around 3–6 nm and 10–12 nm. The MC possesses a high BET specific surface area of 1800 m^2 g^{-1}, along with a pore volume of 0.5 cm^3 g^{-1}. After loading with Cu and S, the N_2 sorption isotherms of both MC-Cu and MC-Cu-S still maintain type I isotherm, but the total amount of the adsorbed N_2 and the pore size are reduced. As depositing with Cu, the BET specific surface area is reduced from 1800 m^2 g^{-1} to around 1650 m^2 g^{-1} and the micropore volume is reduced to 85% of initial value. The 10–12 nm pores are filled with Cu, the 3–6 nm is reduced to 2–5 nm. After S impregnation, the most of pores are filled with S, further reducing BET specific surface area to 100 m^2/g and the pore volume to around 0.1 cm^3 g^{-1}. The remained pore room can provide free space for volume change of S/polysulfides during charge and discharge in the Li–S battery.

2.2. Thermal Analysis

The S contents of pure S, MC-S, and MC-Cu-S were measured using thermogravimetry (TGA) and compared in **Figure 4**. Different from the evaporation of pure S in a temperature range of 180 to 300 °C, TGA curve of MC-S composite exhibits two-step in thermal evaporation of S. The first weight loss in the temperature range of 180 to 300°C releases about 22% of S, which mainly attributes to the evaporation of S covered on the external surface of MC, while the second one ranges to around 450 °C and corresponds to release of the rest S (≈28%) inside the pores of MC. The two-step S-loss curves were also reported in carbon-S composites synthesized by melting S infiltration method.[35] Due to the bonding between Cu and S, S starts to release from the MC-Cu-S composite at about 300 °C and all of the S (≈50%) can be evaporated until the temperature reaches to approximate 500 °C. The delay in releasing S from MC-Cu-S composite confirms that S is indeed stabilized by Cu nanoparticles in the MC-Cu-S composite, which is attributed to the strong interaction between Cu and S.

2.3. Electrochemical Properties

The first three charge/discharge profiles of the MC-S and MC-Cu-S electrodes at 100 mA g^{-1} are shown in **Figure 5**. The first

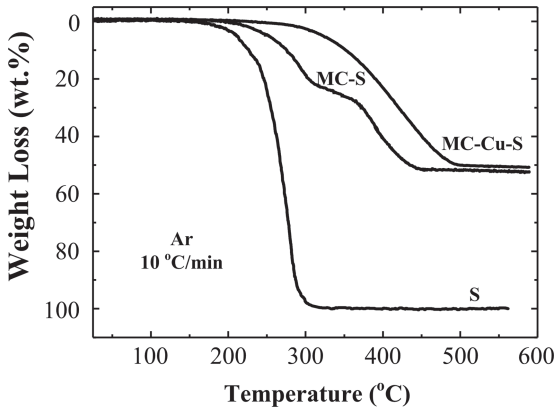

Figure 4. TGA curves for the samples of pure S, MC-S, and MC-Cu-S.

charge/ discharge curves of the MC-S electrode show a short high voltage plateau at 2.4 V (vs Li/Li^+) followed by a long low-voltage at 1.0 to 1.3 V in the discharge and only one plateau at 2.3 V (vs Li/Li^+) in the charge (Figure 5a). In the second discharge, the short high voltage plateau at 2.4 V (vs Li/Li^+) vanished and only one long plateau of 1.5 V can be observed. The disappear of high voltage plateau is attributed to the lack of high-order polysulfides and the low voltage lithiation plateau is probably due to the bonding between Li_xS and Cu.[24,25] The lithiation capacity is around 1050 mAh g^{-1} in the first cycle, but the capacity drops quickly to approximately 465 mAh g^{-1} in the second cycle and further to 250 mAh g^{-1} in the third cycle for the MC-S cathode. As for the MC-Cu-S electrode, its potential plateaus are almost identical to those of the MC-S, but higher reversible capacities can be obtained after the first cycle. The lithiation capacity is around 710 mAh g^{-1} in the second cycle and about 600 mAh g^{-1} in the third cycle. Obviously, the first discharge voltage profiles of MC-S electrode and MC-Cu-S electrode show an arched shape in the range from 100 to 1000 mAh g^{-1}. It is no surprise, since high S loading, at first fast volume change will cause large strain/stress during initial lithiation process, which requires a large overpotential. After relaxation of the strain/stress through expansion of pore size of high surface area MC, the overpotential is reduced in the following discharge. The initial three lithiation/delithiation behaviors of the MC-S and MC-Cu-S electrodes were also characterized using cycle voltammetry (Figure 5). Considering that the cathodic peak corresponding with the low plateaus observed in the first lithiation for MC-S and MC-Cu-S would not be completely visualized during cyclic voltammetry (CV) measurement, a wider voltage window of 0.7–3.0 V was employed in the first cycle scan. The MC-S electrode exhibits a small cathodic peak at about 2.4 and a large peak starts at 1.7 V (centred at 0.8 V) in the first cycle as shown in Figure 5c. The small peak at high voltage of 2.4 V (vs Li/Li^+) is associated to the formation of soluble high-order polysulfides (Li_2S_x, $4 \le x \le 8$) during lithiation, while the low-voltage peak is related to formation of insoluble low-order polysulfides Li_2S_2 and/or Li_2S. The cathodic peak at 2.4 V (vs Li/Li^+) vanishes in the second cycle, suggesting that high-order polysulfides dissolve into (or react with) electrolyte (1.0 M $LiPF_6$ + EC/DEC (1 : 1 v/v)). However, after the first cycle, the current of the low-voltage peak reduced and the peak-voltage shifted toward more positive direction (around 1.5 V). The same CV behaviour also reported in high capacity Si and metal oxide electrodes.[54] The low voltage in the first lithiation scan is attributed to large strain/stress due to large volume change requiring a large overpotential, while in the second lithiation, the strain/stress was reduced due to the introduction of large defects in the electrode and pore size expansion of carbon in the first lithiation, and thus reducing the overpotential and shifting the voltage to a high value in the second lithiation.[51] The reduction of the current for the lithiation peak in the second cycle is due to the dissolution of high-order polysulfide.[33,55] For anodic scan, only one broad peak at 2.3 V (vs Li/Li^+) associating with oxidation of Li_2S back to polysulfide can be observed. The currents of both the cathodic and the anodic peaks decrease slightly in third cycle as compared to those of in the second cycle, which may arise from the dissolution of polysulfides. While for the MC-Cu-S, the CV profiles is almost identical to that of the MC-S, but the peak current of MC-Cu-S at 2.4 V (vs Li/Li^+) in the first (cathodic) discharge is lower than that of MC-S (see Figure 5d), demonstrating that S_8 content in MC-Cu-S is lower than that in MC-S sample. In addition, the peak voltage related to conversion from low-order polysulfide to Li_2S for MC-Cu-S is higher than those of MC-S owing to high conductivity of the MC-Cu-S material.

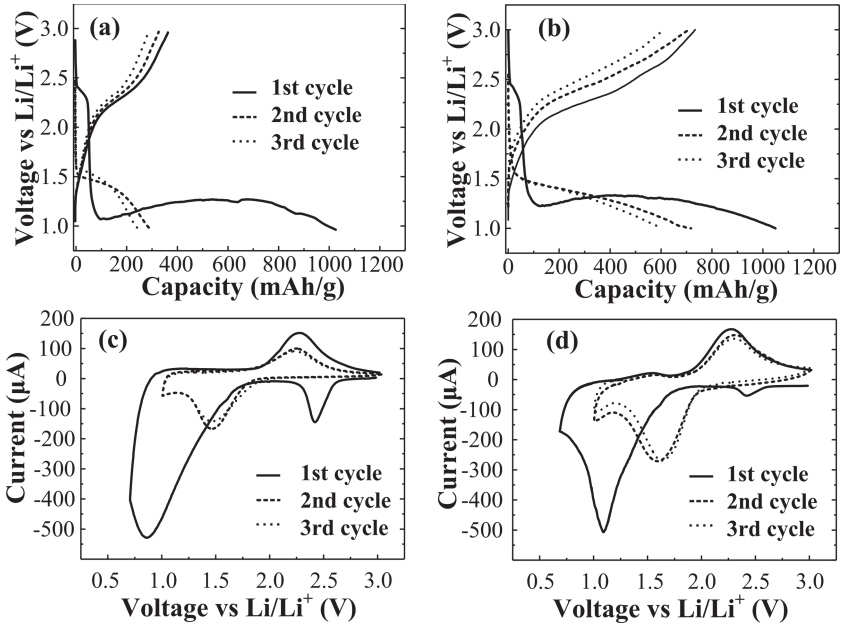

Figure 5. Discharge/charge voltage profiles and cyclic voltammograms of the electrodes in the first three cycles at 100 mA g^{-1}: a,c) the MC-S electrode, and b,d) the MC-Cu-S electrode. The voltage windows in the cyclic voltammograms are 0.7–3.0 V for the first cycle and 1.0–3.0 V for the 2nd and 3rd cycle.

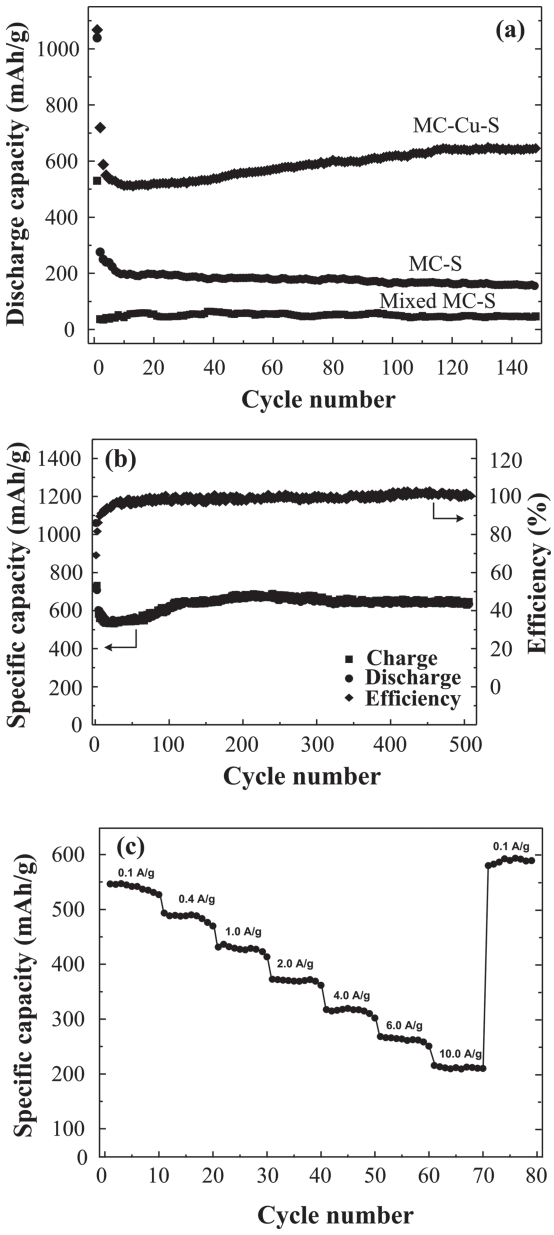

Figure 6. a) Discharge capacity curves of Mixed MC-S, MC-S, and MC-Cu-S composite electrodes in 150 cycles at a current density of 100 mA g^{-1}. b) Cycling performance and Coulombic efficiency of the MC-Cu-S composite electrode. c) Rate capability behavior of the MC-Cu-S composite electrode at different current density from 0.1 A g^{-1} to 10.0 A g^{-1}.

The charge/discharge cycling stability of the Mixed MC-S, MC-S and MC-Cu-S composite electrodes are compared in **Figure 6**(a). The initial discharge capacity of the Mixed MC-S cathode is only around 520 mAh g^{-1}, far less than the theoretical value; after the initial cycle, the capacities drop to less than 100 mAh g^{-1}. The low capacity is not surprising because 1) the low conductive S_8 is not uniformly distributed into the MC matrix and 2) the polysulfide anions react with carbonate solvent-based electrolyte (1.0 M $LiPF_6$ + EC/DEC (1 : 1 v/v).[40] For the S impregnated sample of MC-S, a high discharge capacity of 1050 mAh g^{-1} is obtained in the first cycle, but the capacity reduces to only 300 mAh g^{-1} in the second cycle, and the capacity continuously decreases and stabilizes 150 to 200 mAh g^{-1} after the tenth cycles. The capacity decay in the first ten cycles is probably due to the dissolution of lithium polysulfide intermediates (Li_2S_x, $4 \le x \le 8$) in electrolyte and the reaction between highly reactive lithium polysulfide anions and carbonated electrolyte. As for the MC-Cu-S composite electrode, the initial discharge capacity is almost similar to that of the MC-S sample. The capacity drops to 550 mAh g^{-1} in initial ten cycles, then the capacity starts to gradually increase after undergoing around 50 cycles, and finally restores back to more than 600 mAh g^{-1} after 110 cycles and maintains around 630 mAh with progressive cycling to 500 cycles. (see Figure 6b). Additionally, the Coulumbic efficiency at a current density of 100 mA g^{-1} closes to 100% after ten cycles as shown in Figure 6b. The similar phenomena of capacity drop and recover during charge/discharge cycling were also reported for the study of graphene-62.5% S composite cathode by Sun and co-workers and bulk mesoporous carbon-50% S cathode by Nazar's group.[41,56] This is probably related to high S loading requiring an initial activation process.[47] The large capacity difference between MC-Cu-S and MC-S demonstrates that 10% of Cu loading can greatly enhance the capacity and cycling stability of MC-S cathodes. Obviously, the strong interaction between Cu and S and high electronic conductivity of Cu largely increase the S utilization even when S loading reaches to 50%. Most of all, the interaction between Cu and S improves the cycling stability of the S cathode in the low-cost carbonate-based electrolyte. Use of small amount of metal to stabilize S composite cathode in carbonate electrolyte opens a new window to develop low-cost S-based cathodes for EV and renewable energy storage.

The rate capability behaviors of the MC-Cu-S nanocomposite electrode in current density range from 0.1 A g^{-1} to 10.0 A g^{-1} are also shown in Figure 6c. A reversible capacity of 420, 360, and 300 mAh g^{-1} can be obtained at 1.0, 2.0, and 4.0 A g^{-1}, respectively, owing to the good electrical conductivity of MC-Cu matrix. Even at high rate up to 10.0 A g^{-1}, a capacity of 200 mAh g^{-1} can still be obtained. The capacity of about 600 mAh g^{-1} can be retained when the rate is reduced back to 0.1 A g^{-1} after 70 cycles, showing a great merit for an abuse tolerance of Li–S battery with varied current densities. Simply adding 10% of Cu into carbon-based S nanocomposite electrodes can also improve the rate performance of S-based cathode with 50% content.

Although only few studies on microporous carbon as S host was reported[23] due to the less effect in confining polysulfies, the microporous carbon can become an ideal S host after Cu deposition since the micropores allow Cu nanoparticles to be deposited inside and the Cu deposition into the micropores reduces the pore size. The combination of chemical bonding Cu-S and physical confinement of Cu-decorated micropores effectively reduces the shuttle reaction. Therefore, the MC-Cu-S cathodes show stable, high and reversible capacities together with good rate and cycling capabilities in commercial carbonate-based electrolyte. The mechanism for the exceptional performance of this MC-Cu-S cathode is schematically demonstrated in **Figure 7**. The MC possesses uniform microprous structure in pristine state (Figure 7a). After chemical deposition of Cu and solution wetting-infusion of S, the Cu nanoparticles

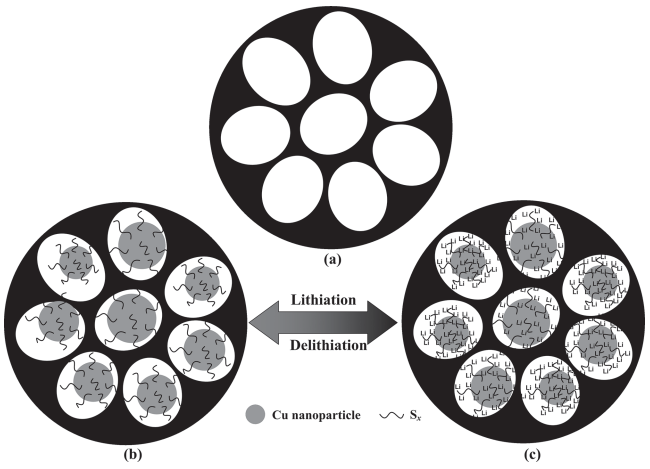

Figure 7. Schematic illustration of lithiation/delithiation process of the MC-Cu-S cathode.

percolate throughout the MC host acting as anchor to stabilize the S and formed Li_xS during lithiation (Figure 7b), and delithiation (Figure 7c). Combined effects of physical confinement by porous carbon matrix and chemical bonding between Cu and Li_xS effectively reduce the shuttle reaction. In addition, the micropores in the MC provide free space for volume change of S and polysulfides, as evidenced by the MC-S with higher cycling capacities as compared to the Mixed MC-S sample.

In summary, by combining with inherent microporous structure of MC, this Cu nanoparticle decorated MC material provides superior confinement ability for S and polysulfides, a sufficient space to accommodate S volumetric expansion, a large contact area with the S, and a short transport pathway for both electrons and Li^+, and thus resulting in effectively stabilizing the S cathode with high S loading in low-cost carbonate solvent-based electrolyte and significantly increasing its utilization, finally demonstrating excellent electrochemical performance of S-based cathode.

3. Conclusions

The ultrasonic-assisted multiple wetness impregnation and synchro-dry technique was employed to prepare a composite with small amount (10%) of Cu additive in microporous carbon. The Cu nanoparticles loading in MC can effectively stabilize the heavy S loaded in MC-Cu-S cathode using a low-cost carbonate-based electrolyte. The unique structural MC-Cu-S composite cathode containing 50% S shows Coulumbic efficiency close to 100%, maintains capacities of around 630 mAh g^{-1} at the current density of 100 mA g^{-1} with progressive cycling up to 500 cycles, and provides a capacity of 200 mAh g^{-1} even at a high rate of 10.0 A g^{-1}. The exceptional performance of MC-Cu-S cathode is because: i) Cu nanoparticles chemically stabilize S by formation of solid Cu-polysulfide clusters through strong interaction between Cu and S. The Cu-polysulfide clusters reduce the amounts of S_8 and high-order polysulfides, allowing carbonate-based electrolytes to be used; ii) Cu nano-inclusions enhance the electronic conductivity of the MC-Cu-S cathodes; iii) MC host provides free space for volume change of S/polysulfides. The results represent that small amount of metal nanoparticle anchored in MC can substantially stabilize the S cathode, increasing the S loadings and improving the cycling stability.

4. Experimental Section

Synthesis of MC-Cu: A commercial microporous carbon (MC) (ACS Material LLC, USA) with high surface area was selected as the matrix to support active materials and used as received. Copper dinitrate ($Cu(NO_3)_2$, Sigma-Aldrich, 98%) was first dissolved in ethanol alcohol (Aldrich 98%) to form a 50% $Cu(NO_3)_2$ content solution ($Cu(NO_3)_2$/EtOH-solution). An ultrasonic-assisted multiple wetness impregnation and synchro-dry method was applied to load Cu dinitrate in MC, i.e. the copper dinitrate solution was first added to MC and subsequently sonicated with a Branson Sonifier S-450A at 60 °C to evaporate the solvent. This process was repeated until a certain amount of $Cu(NO_3)_2$ was added to MC. The resulting sample was then reduced at 200 °C for 1 h with a heating rate of 5 °C min^{-1} under argon mixed with 5% hydrogen environment. The MC-Cu with different content of Cu can be prepared by adjusting the amount of $Cu(NO_3)_2$ addition. Our previous experiments found the MC deposited with 10% Cu has the best stabilizing effect for S in Li–S batteries among 5, 15, and 20% Cu. Therefore, the MC-Cu material with 10% Cu was synthesized and used in this experiment.

Preparation of MC-Cu-S Nanocomposite: The MC-Cu-S composite was obtained by simple impregnation and drying techniques. The procedure is schematically shown in Scheme 1. S (Sigma-Aldrich) was first dissolved in carbon disulfide (CS_2, Aldrich 98%) to form a 50% S content solution (S/CS_2-solution). 1 g as-obtained MC-Cu powder was added to 2 g of the 50% S-CS_2 solution. The ultrasonic-assisted multiple wetness impregnation and synchro-dry technique was also employed to deposit S. The resulting sample was dried at 60 °C in a vacuum for 24 h, and around 50% of S was loaded into the as-prepared composite. Identical to the MC-Cu-S composite preparation procedure, a sample with 50% of S direct-impregnating into the MC was also prepared (denoted as MC-S hereafter). In addition, a physical mixture of MC and S (denoted as Mixed C-S hereafter) corresponding to the 50% of S in MC were also prepared as a reference sample. To obtain the actual S content in the S-containing samples, thermogravimetry (TGA) was performed on a Netzsch STA 409 PC, Germany, with a heating rate of 10 °C min^{-1}, and highly pure Ar as the purge gas.

Structural Characterization: X-ray diffraction (XRD) patterns were recorded on Rigaku D/max 2400, Japan, with Cu Kα radiation in the 2-Theta range from 10–80°. X-ray photoelectron spectroscopy (XPS) data were collected at room temperature with a Kratos Analytical spectrometer and monochromatic Al Kα (1486.6 eV) X-ray source. Scanning electron microscopy (SEM) images were obtained on a Hitachi S-4700, Japan, operating at 15 kV and equipped with an energy dispersive X-ray spectrometry (EDS). The TEM samples were examined in a JEM 3010 microscope. High spatial resolution imaging and microanalysis were performed with an FEI Titan 80–300 analytical scanning transmission electron microscope (STEM) operated at 300 kV accelerating voltage and equipped with a Fischione Instruments model 3000 high-angle annular dark-field (HAADF) detector and an EDAX lithium-drifted silicon X-ray energy-dispersive spectrometer (XEDS).

Electrochemical Measurements: The S-containing composite was mixed with acetylene black and sodium carboxymethyl cellulose binder in a weight ratio of 80 : 10 : 10, with distilled water as a dispersant. The slurry was coated on an aluminum foil to obtain a film with approximately 80 μm thickness and dried in a vacuum oven at 100 °C overnight. The active material loading was around 1 mg cm^{-2}. The half cells were assembled in a glove box filled with high pure Ar. Lithium metal was used as the counter electrode and reference electrode. The separator was microporous polypropylene Celgard 3501 (Celgard, LLC Corp., USA). The electrolyte was 1.0 M $LiPF_6$ in a mixture of ethylene carbonate/dimethyl carbonate (EC/DEC, 1 : 1 v/v). The charge and discharge

performances of the half-cells were tested with using Arbin battery test station (BT2000, Arbin Instruments, USA) and potential range was controlled between 1.0 and 3.0 V at ambient temperature. The specific capacity was calculated on the basis of the active S material obtained from TGA measurement. The cyclic voltammetry (CV) measurement was conducted with a Gamry Reference 3000 (Gamry Co., USA) at a scan rate of 0.1 mV s^{-1}.

Acknowledgements

The authors gratefully acknowledge the support of the Army Research Office under Contract No.: W911NF1110231 (Dr. Robert Mantz, Program Manager) and the National Science Foundation of China (No. 51272157). The authors acknowledge the support of the Maryland NanoCenter and its NispLab. The NispLab is supported in part by the NSF as a MRSEC Shared Experimental Facility.

Certain commercial equipment, instruments, or materials are identified in this work. Such identification does not imply recommendation or endorsement by the National Institute of Standards and Technology, nor does it imply that the products identified are necessarily the best available for the purpose.

Note: The order of the affiliations was changed after initial online publication.

Received: December 13, 2013
Revised: January 20, 2014
Published online: March 24, 2014

[1] D. Herbert, J. Ulam, *US Patent 3043896*, **1962**.
[2] E. Peled, A. Gorenshtein, M. Segal, Y. Sternberg, *J. Power Sources* **1989**, *26*, 269.
[3] P. G. Bruce, S. A. Freunberger, L. J. Hardwick, J.-M. Tarascon, *Nat. Mater.* **2012**, *11*, 19.
[4] X. Ji, L. F. Nazar, *J. Mater. Chem.* **2010**, *20*, 9821.
[5] A. Manthiram, Y. Fu, Y. Su, *Acc. Chem. Res.* **2013**, *46*, 1051.
[6] C. Barchasz, F. Molton, C. Duboc, J. Lepretre, S. Patoux, F. Alloin, *Anal. Chem.* **2012**, *84*, 3973.
[7] Y. Diao, K. Xie, S. Xiong, X. Hong, *J. Electrochem. Soc.* **2012**, *159*, A421.
[8] Y. V. Mikhaylik, J. R. Akridge, *J. Electrochem. Soc.* **2004**, *151*, A1969.
[9] Y. Yang, G. Zheng, Y. Cui, *Chem. Soc. Rev* **2013**, *42*, 3018.
[10] M. Song, E. J. Cairns, Y. Zhang, *Nanoscale* **2013**, *5*, 2186.
[11] Y. Jung, S. Kim, *Electrochem. Commun.* **2007**, *9*, 249.
[12] L. Suo, Y. Hu, H. Li, M. Armand, L. Chen, *Nat. Commun.* **2013**, *4*, 1481.
[13] D. Aurbach, E. Pollak, R. Elazari, G. Salitra, C. S. Kelley, J. Affinito, *J. Electrochem. Soc.* **2009**, *156*, A694.
[14] Y. Fu, A. Manthiram, *Chem. Mater.* **2012**, *24*, 3081.
[15] J. Fanous, M. Wegner, J. Grimminger, A. Andresen, M. R. Buchmeiser, *Chem. Mater.* **2011**, *23*, 5024.
[16] J. Guo, Y. Xu, C. Wang, *Nano Lett.* **2011**, *11*, 4288.
[17] S. Zheng, Y. Chen, Y. Xu, F. Yi, Y. Zhu, Y. Liu, J. Yang, C. Wang, *ACS Nano* **2013**, *7*, 10995.
[18] W. Zheng, Y. Liu, X. Hu, C. Zhang, *Electrochim. Acta* **2006**, *51*, 1330.
[19] S. Dorfler, M. Hagen, H. Althues, J. Tubke, S. Kaskel, M. J. Hoffmann, *Chem. Commun.* **2012**, *48*, 4097.
[20] L. Ji, M. Rao, H. Zheng, L. Zhang, Y. Li,W. Duan , J. Guo, E. J. Cairns, Y. Zhang, *J. Am. Chem. Soc.* **2011**, *133*, 18522.
[21] H. Wang, Y. Yang, Y. Liang, J. T. Robinson, Y. Li, A. Jackson, Y. Cui, H. Dai, *Nano Lett.* **2011**, *11*, 2644.
[22] Y. Cao, X. Li, I. A. Aksay, J. Lemmon, Z. Nie, Z. Yang, J. Liu, *Phys. Chem. Chem. Phys.* **2011**, *13*, 7660.
[23] B. Zhang, X. Qin, G. Li, X. Gao, *Energy Environ. Sci.* **2010**, *3*, 1531.
[24] C. Zhang, H. Wu, C. Yuan, Z. Guo, X. D. Lou, *Angew. Chem. Int. Ed.* **2012**, *51*, 9592.
[25] J. Kim, D. Lee, H. Jung, Y. Sun, J. Hassoun, B. Scrosati, *Adv. Funct. Mater.* **2013**, *23*, 1076.
[26] N. Jayaprakash, J. Shen, S. S. Moganty, A. Corona, L. A. Archer, *Angew. Chem. Int. Ed.* **2011**, *50*, 1.
[27] C. Liang, N. J. Dudney, J. Y. Howe, *Chem. Mater.* **2009**, *21*, 4724.
[28] X. Li, Y. Cao, W. Qi, L. V. Saraf, J. Xiao, Z. Nie, J. Mietek, J. Zhang, B. Schwenzer, J. Liu, *J. Mater. Chem.* **2011**, *21*, 16603.
[29] X. Ji, K. T. Lee, L. F. Nazar, *Nat. Mater.* **2009**, *8*, 500.
[30] X. Ji, S. Evers, R. Black, L. F. Nazar, *Nat. Commun.* **2011**, *2*, 325.
[31] G. Zhou, D. Wang, F. Li, P. Hou, L. Yin, C. Liu, G. Lu, I. R. Gentle, H. Cheng, *Energy Environ. Sci.* **2012**, *5*, 8901.
[32] W. Weng, V. G. Pol, K. Amine, *Adv Mater.* **2013**, *25*, 1608.
[33] J. Schuster, G. He, B. Mandlmeier, T. Yim, K. T. Lee, T. Bein, L. F. Nazar, *Angew. Chem. Int. Ed.* **2012**, *51*, 3591.
[34] P. G. Bruce, L. J. Hardwick, K. M. Abraham, *MRS Bull* **2011**, *36*, 506.
[35] L. Ji, M. Rao, S. Aloni, L. Wang, E. J. Cairns, Y. Zhang, *Energy Environ. Sci.* **2011**, *4*, 5053.
[36] B. Ding, C. Yuan, L. Shen, G. Xu, P. Nie, X. Zhang, *Chem. Eur. J.* **2013**, *19*, 1013.
[37] G. He, X. Ji, L. F. Nazar, *Energy Environ. Sci.* **2011**, *4*, 2878.
[38] S. Zhang, J. A. Read, *J. Power Sources* **2012**, *200*, 77.
[39] J. Guo, Z. Yang, Y. Yu, H. D. Abruna, L. A. Archer, *J. Am. Chem. Soc.* **2013**, *135*, 763.
[40] J. Schuster, G. He, B. Mandlmeier, T. Yim, K. Tae Lee, T. Bein, L. F. Nazar, *Angew. Chem. Int. Ed.* **2012**, *51*, 3591.
[41] B. Li, W. Wamg, Z. Fu, A. Wang, K. Yuan, *Adv. Mater. Res.* **2006**, *11*, 407.
[42] J. Wang, J. Yang, J. Xie, N. Xu, *Adv. Mater.* **2002**, *14*, 963.
[43] Y. Wang, J. Wu, Y. Tang, X. Lu, C. Yang, M , Qin, F. Huang, X. Li, X. Zhang, *ACS Appl. Mater. Interfaces* **2012**, *4*, 4246.
[44] S. Han, H. Kim, M. Song, P. S. Lee, J. Lee, H. Ahn, *J. Alloys Compd.* **2003**, *349*, 290.
[45] Y. Wang, X. Zhang, P. Chen, H. Liao, S. Cheng, *Electrochim. Acta* **2012**, *80*, 264.
[46] R. Cai, J. Chen, J. Zhu, C. Xu, W. Zhang, C. Zhang, W. Shi, H. Tan, D. Yang, H. H. Hng, T. M. Lim, Q. Yan, *J. Phys. Chem. C* **2012**, *116*, 12468.
[47] Y. Du, Z. Yin, J. Zhu, X. Huang, X. Wu, Z. Zeng, Q. Yan, H. Zhang, *Nat. Commun.* **2013**, *3*, 1177.
[48] R. Steudel, Elemental Sulfur, Sulfur-Rich Compounds II, Springer-VerlagBerlin Heidelberg NY, USA **2003**.
[49] H. Wei, Z. Ye, M. Li, Y. Su, Z. Yang, Y. Zhang, *CrystEngComm* **2011**, *13*, 2222.
[50] C. Chusuei, M. Brookshier, D. Goodman, *Langmuir* **1999**, *15*, 2806.
[51] V. Krylova, M. Andrulevicius, *Int. J. Photoenergy* **2009**, DOI:10.1155/2009/304308.
[52] V. Toniazzo, C. Mustin, J. Portal, B. Humbert, R. Benoit, R. Erre, *Appl. Surf. Sci.* **1999**, *143*, 229.
[53] G. Greczynski, Th. Kugler, W. Salaneck, *Thin Solid Film* **1999**, *354*,129.
[54] U. Kasavajjula, C. Wang, A. J. Appleby, *J. Power Sources* **2007**, *163*, 1003.
[55] J. Guo, Q. Liu, C. Wang, M. R. Zachariah, *Adv. Funct. Mater.* **2012**, *22*, 803.
[56] H. Sun, G. Xu, Y. Xu, S. Sun, X. Zhang, Y. Qiu, S. Yang, *Nano Res.* **2012**, *5*, 726.